IOP PUBLISHING PHYSICS IN MEDICINE AND BIOLOGY

Phys. Med. Biol. **52** (2007) 5309–5327 doi:10.1088/0031-9155/52/17/014

Probabilistic forward model for electroencephalography source analysis

Sergey M Plis[1,2], John S George[1], Sung C Jun[1], Doug M Ranken[1], Petr L Volegov[1] and David M Schmidt[1]

[1] MS-D454, Applied Modern Physics Group, Los Alamos National Laboratory, Los Alamos, NM 87545, USA
[2] Department of Computer Science, University of New Mexico, Albuquerque, NM 87131, USA

E-mail: pliz@cs.unm.edu

Received 7 June 2007, in final form 19 July 2007
Published 16 August 2007
Online at stacks.iop.org/PMB/52/5309

Abstract

Source localization by electroencephalography (EEG) requires an accurate model of head geometry and tissue conductivity. The estimation of source time courses from EEG or from EEG in conjunction with magnetoencephalography (MEG) requires a forward model consistent with true activity for the best outcome. Although MRI provides an excellent description of soft tissue anatomy, a high resolution model of the skull (the dominant resistive component of the head) requires CT, which is not justified for routine physiological studies. Although a number of techniques have been employed to estimate tissue conductivity, no present techniques provide the noninvasive 3D tomographic mapping of conductivity that would be desirable. We introduce a formalism for probabilistic forward modeling that allows the propagation of uncertainties in model parameters into possible errors in source localization. We consider uncertainties in the conductivity profile of the skull, but the approach is general and can be extended to other kinds of uncertainties in the forward model. We and others have previously suggested the possibility of extracting conductivity of the skull from measured electroencephalography data by simultaneously optimizing over dipole parameters and the conductivity values required by the forward model. Using Cramer–Rao bounds, we demonstrate that this approach does not improve localization results nor does it produce reliable conductivity estimates. We conclude that the conductivity of the skull has to be either accurately measured by an independent technique, or that the uncertainties in the conductivity values should be reflected in uncertainty in the source location estimates.

(Some figures in this article are in colour only in the electronic version)

1. Introduction

Electroencephalography (EEG) source analysis is strongly affected by the geometric and parametric accuracy of the forward model (Hämäläinen *et al* 1993). Just as forward model accuracy is important for EEG source analysis in isolation (Ollikainen *et al* 1999, Marin *et al* 1998), it is especially important for integrated MEG/EEG source analysis. An inaccurate forward model may result in incompatibility between MEG and EEG analysis results. Since MEG is less sensitive to forward model parameters than EEG, combined analysis might lead to a less accurate result, defeating one purpose of joint analysis.

In contrast to magnetoencephalography (MEG), where a relatively simple forward model (Sarvas 1987) yields adequate inverse results under a wide range of situations, EEG demands more detailed and sophisticated forward models (Hämäläinen and Sarvas 1989) for similarly accurate inverse results. More realistic models introduce new parameters, which need to be estimated accurately for the models to work properly. However, the estimation of conductivity parameters is a difficult process and inaccuracies introduce uncertainties into forward computations. EEG is highly sensitive to the effects of head geometry and conductivity profile on the flow of extracellular currents that give rise to potentials at the head surface. Sources of uncertainty include the difficulties of precisely estimating the head shape, skull structure, and the structure and anisotropy of white and gray matter (Ollikainen *et al* 1999). Gross structural information can be obtained from MRI and CT scans and then incorporated into the forward model. However, it is much harder, and at the same time very important, to use information about the finer structure of the skull.

Leahy and colleagues (Leahy *et al* 1998) conducted a series of experiments on a human skull phantom. These studies showed that, on average, the localization error over 32 dipoles was 7–8 mm for EEG and 2–3 mm for MEG. This is an important practical observation. In principle, under the assumption that there are no forward model errors, the expected performance of EEG for the localization of a small number of sources is compatible to that of MEG, as demonstrated in Liu *et al* (2002). The authors of Leahy *et al* (1998) conclude that the biggest source of error in the skull is the uncertainty introduced when current passes through the bone. The diploic space of the skull is a relatively conductive structure, which can greatly affect the flow of volume currents in the head. The diploic space structure is located in much of the cranium with only a few exceptions such as the temporal lobes, but the thickness of the diploid varies. Several researchers have suggested that a more accurate model, which considers the effects of the diploic space, can lead to better localization. In principle, finite element (FEM) and finite difference (FD) models can describe the fine details of the skull including realistic geometry, variable conductivity and even anisotropy (Strang and Fix 1973). Unfortunately, their heavy computational load is a drawback for the use in iterative methods, which require numerous evaluations of the forward solution. These methods require a precomputing step (mesh generation and stiffness matrix construction) and the actual solution step, which is usually performed using efficient sparse solvers but still requires a lot of time for the meshes needed for an accurate result.

The increased computational complexity needed to account for all details of diploic space may not deliver the expected benefits because of the difficulties in obtaining the detailed information needed to construct such a model. Uncertainties in identifying and characterizing fine-scale geometrical structures can, in principle, be eliminated by using high resolution CT. Unfortunately, the ionizing radiation associated with x-ray techniques prevents the routine use of this approach. Other currently existing 'safe' methods do not have the resolution needed to accurately reflect details of the spongiosa. The noninvasive estimation of conductivity profiles using methods such as diffusion tensor imaging (DTI) (Tuch *et al* 2001)

does not provide the resolution and reliability required to describe the fine details of the diploic space. Our experience suggests that the DTI method is more useful for characterizing anisotropy in tissue conductivity than direct measurement of tissue conductivity. Even if accurate conductivity estimates can be obtained, numerical problems, arising from using a fine scale mesh to model the diploic space, can limit accuracy. The continuing development of noninvasive impedance tomography methods driven by the demand to characterize finer structures and obtain detailed information about the brain may eventually allow the collection of detailed conductivity information. However, numerical problems can limit the effectiveness of conductivity estimation.

Boundary element method (BEM) models are less computationally intensive compared to FEM models, while providing improved computational accuracy relative to simple analytical models. An accurate modeling of the major conductivity boundaries within the head geometry together with smaller computational complexity makes BEM models a valuable tool in iterative methods, even though they do not capture all the details possible in FEM models.

The ratio of conductivities between adjacent compartments plays an important role in BEM calculations. The average values of scalp, brain and cerebrospinal fluid conductivities are relatively easy to obtain and are well accepted in the community. The quantity that affects the ratios and thus the results of computations is the skull average conductivity. Traditionally the value of 80:1 for the brain-to-skull ratio (Rush and Driscoll 1969) is used in EEG forward calculations. Another popular ratio is 100:1. However, recent findings show that the living skull has much higher conductivity. Indirect measurements by electrical impedance tomography (EIT) (Oostendorp *et al* 2000) obtained a ratio of 15:1. A recent result (Hoekema *et al* 2003) uses live skull measurements of the bone removed during temporal lobe epilepsy surgery and obtained a ratio of 5:1. Baysal and Haueisen (2004) obtained a ratio of 23:1. Fine measurements where inner, outer and diploic space layers were measured separately were performed in Akhtari *et al* (2002). Notably, reported values are consistently higher than the value of Rush and Driscoll (1969) but disagree with each other. Difficulties with obtaining an exact value for the average conductivity of the skull introduces uncertainty into forward calculations.

Taking any average value as a basis for the forward model leads to unaccounted differences from subject to subject. *In vivo* measurements of individuals can partially solve the problem by providing subject-dependent data but measurement errors associated with this approach introduce uncertainty and such studies are difficult to conduct on a routine basis with existing EEG equipment. It is important to understand this uncertainty and propagate it to the result in order to have some confidence bounds on the solution and have results that are consistent with the underlying source.

In the longer term, the best strategy for producing accurate forward models for EEG is likely to be some form of EIT. The usual strategy for EIT is to apply current between pairs of electrodes at the head surface while measuring the modulation of potential at other surface electrodes. However, these surface based measurements suffer from much of the ill-posed character associated with the inverse problem of source localization. While general tomographic reconstruction is limited in performance and accuracy, several investigators have reported good results by constraining the geometry of the various classes of tissue based on medical image data, and fitting a small number of class impedance values based on EIT data (Glidewell and Ng 1997, Salman *et al* 2005). However, the highly resistive skull limits most of the current to the superficial layers or the head (e.g. the scalp) so that measurements carry relatively little information about the skull and cortical conductivity. This might be addressed by using at least one electrode with preferred access to the interior of the skull, for example though one of the natural penetrations. EIT incorporating MR imaging is potentially

a very powerful techniques. Passing current through a conductive volume will generate local magnetic field perturbations, especially at conductivity boundaries, and these perturb the MRI signal arising from the region. Although recently many investigators have attempted to exploit this idea to directly image neural currents, EIT techniques should relax sensitivity limitations and allow 3D mapping of conductivity without requiring assumptions about tissue structure.

One alternative strategy for measuring the conductivity of the skull is to extract its value from the EEG data by simultaneously optimizing over source parameters and the conductivity. This approach has been suggested in Lew *et al* (2007), Vallaghé *et al* (2007). In section 2 we use Cramer–Rao bounds to demonstrate the impracticality of this approach by showing that the uncertainty in the skull conductivity is inherent to the model. In order to account for this uncertainty we introduce the concept of a probabilistic forward model in section 3. For the purposes of this paper we ignore the uncertainties introduced by the brain structure and leave only the uncertainty due to the skull. Since the evaluation of the model is performed using a human skull phantom, such treatment is valid and helps to demonstrate concepts in a restricted and simpler environment. The notion of a probabilistic forward model is well suited for Bayesian inference with Markov Chain Monte Carlo, which is developed in this framework. Section 4 shows an application of the probabilistic model to simulated data and the data from the human skull phantom experiment (Leahy *et al* 1998). The application and evaluation of results is based on the goal of creating a model that is useful for the joint analysis of MEG and EEG data.

2. Cramer–Rao lower bound

It was suggested in Lew *et al* (2007) that the true value of the ratio of brain to skull conductivity can be estimated from the EEG data by simultaneous optimization over source parameters and the conductivity in a piecewise constant conductivity model. The authors chose a limited number of brain to skull conductivity ratios and performed optimization in the resultant discrete space. Although the study produced correct results in the noiseless case, adding noise has led to the deterioration of accuracy. Similar behavior was observed in Vallaghé *et al* (2007).

In this section, we demonstrate the impracticality of simultaneous optimization over dipole parameters and the skull conductivity. For this, we calculate the Cramer–Rao lower bound (CRLB) on the dipole location for the case where the conductivity of the skull is a parameter and compare the bound with the case where the skull conductivity is fixed (as in Mosher *et al* (1993)). The Cramer–Rao bound we obtained discloses a considerable increase in location uncertainty observed when introducing a parameter for the skull conductivity and explains the fast performance deterioration associated with a decrease in the signal-to-noise ratio observed in Lew *et al* (2007) and Vallaghé *et al* (2007).

The CRLB gives the minimal achievable variance for any unbiased estimator. When calculating the CRLB in this work, we follow the notation and derivations of Mosher *et al* (1993), Stoica and Nehorai (1989). We are interested only in a single time point and a single dipole source. This is sufficient for our purposes of studying the influence of conductivity of the skull on the bound. Thus, we do not develop the general form of a CRLB, as done in, e.g., Mosher *et al* (1993), but just present a special case. As in the aforementioned examples, the bounds are based on the spherical head model, without loss of generality of the formulation.

The EEG forward model for a single time point, i.e. fixed dipole location and orientation, can be represented by

$$\boldsymbol{v} = \mathbf{G}(\boldsymbol{I})\boldsymbol{q} + \boldsymbol{\eta}, \tag{1}$$

where $\boldsymbol{v}$ is the measurement vector, $\mathbf{G}$ is the gain matrix, $\boldsymbol{I}$ and $\boldsymbol{q}$ are the dipole location and moment vectors, and $\boldsymbol{\eta}$ is the noise vector. The parameter vector for this model is

$$\psi = [\nu, \boldsymbol{q}^T, \boldsymbol{I}^T]^T, \tag{2}$$

where ν is the noise variance.

Denoting an unbiased estimate of these parameters by $\widehat{\psi}$, the Cramer–Rao inequality theorem states that the covariance matrix of the errors between the true and the estimated parameters is bounded from below by the inverse of the Fisher information matrix,

$$\mathbf{C} = \mathbf{E}[(\psi - \widehat{\psi})(\psi - \widehat{\psi})^T] \geqslant \mathbf{J}^{-1}, \tag{3}$$

where the Fisher information matrix $\mathbf{J}$ is defined as

$$\mathbf{J} = \mathrm{E}\left\{\left[\frac{\mathrm{d}}{\mathrm{d}\psi}\log \mathrm{P}(\mathbf{M}|\psi)\right]\left[\frac{\mathrm{d}}{\mathrm{d}\psi}\log \mathrm{P}(\mathbf{M}|\psi)\right]^T\right\}. \tag{4}$$

E{} denotes the expected value, and $P(\mathbf{M}|\psi)$ denotes the likelihood with respect to data $\mathbf{M}$. For the regular case of m sensors and a single time instance derived in Mosher *et al* (1993), where σ_{skull} is a fixed value, the Fisher information matrix (repeated from equation (A.12)) is

$$\boldsymbol{J} = \frac{1}{\nu}\begin{bmatrix} \frac{m}{2\nu} & 0 & 0 \\ 0 & \mathbf{G}^T\mathbf{G} & \Delta \\ 0 & \Delta^T & \Gamma \end{bmatrix}. \tag{5}$$

When we add the σ_{skull} parameter to our estimator, the parameter vector becomes

$$\psi = [\nu, \boldsymbol{q}^T, \boldsymbol{I}^T, \sigma_{\text{skull}}]^T \tag{6}$$

and the Fisher information matrix (for derivation details, see appendix A) is expressed as

$$\boldsymbol{J} = \frac{1}{\nu}\begin{bmatrix} \frac{m}{2\nu} & 0 & 0 & 0 \\ 0 & \boldsymbol{G}^T\boldsymbol{G} & \Delta & \alpha_\Delta \\ 0 & \Delta^T & \Gamma & \beta_\Gamma \\ 0 & \alpha_\Delta^T & \beta_\Gamma^T & S \end{bmatrix}. \tag{7}$$

The CRLB for the location parameters is obtained from the inverse of the Fisher information matrix $\boldsymbol{J}$. In $\boldsymbol{J}^{-1}$ the 3×3 submatrix bounding the error covariance of these parameters is located at the place of Γ in the matrix $\boldsymbol{J}$. It is expressed as

$$\boldsymbol{C}(\boldsymbol{I}) = \begin{bmatrix} \sigma_x^2 & \sigma_x\sigma_y & \sigma_x\sigma_z \\ \sigma_y\sigma_x & \sigma_y^2 & \sigma_y\sigma_z \\ \sigma_z\sigma_x & \sigma_z\sigma_y & \sigma_z^2 \end{bmatrix} \tag{8}$$

This error covariance represents an ellipsoid. Following (Mosher *et al* 1993) we consider errors in all directions equally important and focus on the length of the error vector. Thus, the quantity of interest is the root mean square error, which is

$$\mathrm{RMS}(\boldsymbol{I}) = \sqrt{\sigma_x^2 + \sigma_y^2 + \sigma_z^2}. \tag{9}$$

A single parameter for the conductivity of the skull (σ_{skull}) is relevant in the context of the piecewise-constant conductivity models. Such models are called n-shell models. 3- and 4-shell models are the most commonly encountered in EEG source analysis (Berg and Scherg 1994, Sun 1997, Cuffin and Cohen 1979). In this section we use a 4-shell spherical model and the approximation to its analytical solution of Sun (1997). Electrodes are attached to the upper hemisphere in six concentric circles with an additional electrode directly on the top. The first

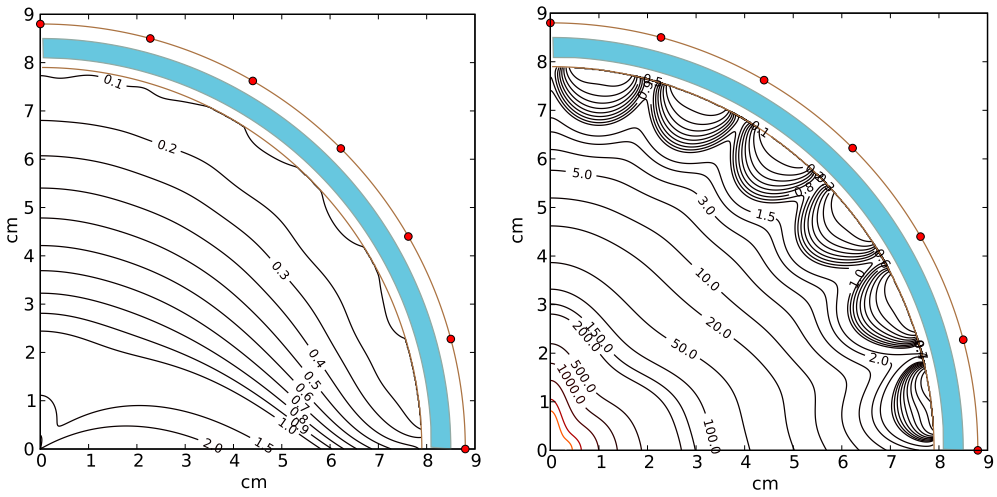

(a) σ_{skull} is fixed (b) σ_{skull} is a parameter

Figure 1. EEG CRLB for a 4-shell model and a tangential dipole living in the displayed plane. The skull shell is displayed with a solid blue color. The noise to dipole strength ratio $\sigma_\nu/\boldsymbol{Q} = 40$ (V A^{-1} m^{-1}). Two estimators are shown: one (on the left) that treats the conductivity of the skull as a fixed number (0.00421/(Ω m)) and the other (on the right) that treats it as a parameter.

circle is placed 15° down from the axis, the rest follow with an interval of 15°. The circles have 6, 12, 18, 24, 30 and 36 electrodes, respectively. Due to the symmetry of this setup we display CRLBs only for a quarter of the sphere projection.

Figure 1 displays CRLB for dipole location as defined in Mosher *et al* (1993) for the cases when σ_{skull} is fixed and for when it is an optimization parameter. A single tangential dipole in the plane of the contour plot was placed at different points and the CRLB was calculated. The dipole strength $\boldsymbol{Q}$ and the noise variance ν were set such that the ratio $\sigma_\nu/\boldsymbol{Q}$ is equal to 40 (V A^{-1} m^{-1}), where σ_ν represents the noise standard deviation. The contour lines in figure 1 represent the lines of constant error variance.

The additional parameter of σ_{skull} in figure 1(b) significantly degrades the bounds. This means that compensating the uncertainty in the measurements of skull conductivity by jointly optimizing over σ_{skull} and location-orientation parameters will not lead to improvements in the result. To the contrary, the location estimation accuracy will significantly deteriorate.

3. Probabilistic forward model

As demonstrated in section 2, simultaneous optimization of the skull conductivity and dipole parameters is impractical. Extracting information about skull conductivity from the data concurrently with dipole parameters impairs the accuracy of the result. It is essential to obtain the skull conductivity in a separate procedure (Salman *et al* 2005, Tidswell *et al* 2001, Glidewell and Ng 1997) lest the accuracy deteriorates considerably. However, existing conductivity measurements do not eliminate all the uncertainties. For example, inter- and intra-subject variability prevents obtaining a single correct result usable in all circumstances. Ignoring this uncertainty by setting some fixed value of the conductivity may adversely affect the result of source analysis. A more appropriate approach is to account for the uncertainty in the computations and propagate it to the result.

In this section we introduce a probabilistic forward model which explicitly accounts for uncertainties in the skull conductivity. The uncertainty in the value of the skull conductivity is modeled by treating this conductivity as a random parameter. Whereas widely used forward models produce identical results given identical input, our model, when sequentially run on identical input, generates a distribution governed by the probability density of the skull conductivity and its nonlinear influence on the forward computation. This is a useful feature for studying the effects of the uncertainty in skull conductivity on the sensor measurements and source localization. Moreover, the probabilistic forward model has great potential as a part of a Monte Carlo based source analysis (Schmidt *et al* 1999, Jun *et al* 2005, 2006, Gelman *et al* 1995, Gilks 1995), because it quantifies the effect of the uncertainty on source analysis results.

We introduce the probabilistic forward model based on a BEM model. In spite of the generality of our approach to treating uncertainty in the forward model parameters, we base our presentation on a BEM model for the reasons listed in the introduction. We first demonstrate how conductivities affect the BEM model. Second, we develop a Bayesian formulation for the problem, making the probabilistic model an explicit part of the analysis. Third, we describe a method of precomputing BEM matrices that speeds up source analysis.

3.1. Dependence on the conductivity

In order to construct the model, we first show how conductivities affect BEM output. The voltage vector $\boldsymbol{v}$ observed on the output nodes is calculated by the linear collocation method (Mosher *et al* 1999) used in the calculation in section 4, and is expressed by the following discretized equation:

$$\left(\| - \mathbf{H} + \frac{1}{M}\mathbb{1}\right)^{-1} \boldsymbol{g} = \boldsymbol{v}, \tag{10}$$

where $\|$ is an identity matrix, $\mathbb{1}$ is the matrix with all elements equal to 1, $\boldsymbol{g}$ is the solution in an unbounded homogeneous medium, $\mathbf{H}$ is the stiffness matrix that includes conductivities of all shells.

For the 3-shell case, $\mathbf{H}$ can be represented as a 9-block matrix where each block B_{ij} depends only on the mesh geometry of the corresponding interacting shells i and j, and is scaled by a coefficient of the form

$$\frac{\sigma_j^- - \sigma_j^+}{\sigma_i^- + \sigma_i^+}, \tag{11}$$

where σ_j^+ and σ_j^- are the conductivities outside and inside, respectively, of shell j. The 9-block matrix of coefficients is

$$\mathbf{H} = \begin{pmatrix} \frac{\sigma_1^- - \sigma_1^+}{\sigma_1^- + \sigma_1^+} & \frac{\sigma_2^- - \sigma_2^+}{\sigma_1^- + \sigma_1^+} & \frac{\sigma_3^- - \sigma_3^+}{\sigma_1^- + \sigma_1^+} \\ \frac{\sigma_1^- - \sigma_1^+}{\sigma_2^- + \sigma_2^+} & \frac{\sigma_2^- - \sigma_2^+}{\sigma_2^- + \sigma_2^+} & \frac{\sigma_3^- - \sigma_3^+}{\sigma_2^- + \sigma_2^+} \\ \frac{\sigma_1^- - \sigma_1^+}{\sigma_3^- + \sigma_3^+} & \frac{\sigma_2^- - \sigma_2^+}{\sigma_3^- + \sigma_3^+} & \frac{\sigma_3^- - \sigma_3^+}{\sigma_3^- + \sigma_3^+} \end{pmatrix}. \tag{12}$$

To make expression (12) easier to use we separate the conductivity coefficients from the geometry dependent component to get two block-diagonal matrices:

$$\Sigma_L = \begin{pmatrix} \frac{1}{\sigma_1^- + \sigma_1^+} & 0 & 0 \\ 0 & \frac{1}{\sigma_2^- + \sigma_2^+} & 0 \\ 0 & 0 & \frac{1}{\sigma_3^- + \sigma_3^+} \end{pmatrix} \tag{13}$$

$$\Sigma_R = \begin{pmatrix} \sigma_1^- - \sigma_1^+ & 0 & 0 \\ 0 & \sigma_2^- - \sigma_2^+ & 0 \\ 0 & 0 & \sigma_3^- - \sigma_3^+ \end{pmatrix}. \tag{14}$$

The simplified version of expression (12) thus is

$$\mathbf{H} = \Sigma_L \widehat{\mathbf{H}} \Sigma_R, \tag{15}$$

where $\widehat{\mathbf{H}}$ is the stiffness matrix part independent of conductivities. The infinite homogeneous solution can also be split in two parts. One part depends on dipole parameters and the head geometry ($\mathbf{R}$, $\mathbf{J}$, $\mathbf{\Theta}$). The other part depends on conductivity scaling factors. Thus, the infinite homogeneous solution factors as $\boldsymbol{g} = 2\Sigma_L \widehat{\boldsymbol{g}}$. Equation (10) now can be modified by substituting expression (15) for $\mathbf{H}$ and introducing the scaling factors:

$$\left[\left(\| - \Sigma_L \widehat{\mathbf{H}} \Sigma_R + \frac{1}{M} \mathbb{1} \right)^{-1} 2\Sigma_L \right] \widehat{\boldsymbol{g}} = \boldsymbol{v}. \tag{16}$$

Equation (16) makes clear the nonlinear dependence of surface potentials $\boldsymbol{v}$ on conductivities. Also it is apparent that the matrix that depends only on geometry $\widehat{\mathbf{H}}$ can be precalculated once. Subsequent changes in skull conductivity would require less computation.

3.2. Bayesian formulation

What follows is built on a previous result for spatiotemporal Bayesian analysis by Jun *et al* (2005). The following notation is needed to define the Bayesian formulation:

$\mathbf{E}$	$T \times L$ matrix representing observed spatiotemporal data. L and T represent the number of sensors and the number of time samples in measurements.
N	*a priori* unknown number of dipole sources
$\mathbf{R} = (R_1, R_2, \ldots, R_N)$	vector of N dipole sources, with each $R_i = (x_i, y_i, z_i)$ representing the location of the ith dipole.
$\mathbf{J} = (J_1, J_2, \ldots, J_N)$	vector of N current time courses, with each $J_i = \left(j_i^1, j_i^2, \ldots, j_i^T\right)$ representing signed dipole moment magnitude over time of the ith dipole. Negative sign means that dipole moment orientation is reversed.
$\mathbf{\Theta} = (\theta_1, \theta_2, \ldots, \theta_N)$	vector of N dipole moment orientations, with each θ_i representing a unit tangential direction of the ith dipole.
σ_{skull}	skull conductivity as used in section 2.

Equation (16) conveniently separates the part depending on the source parameters from the part depending on the skull conductivity. This allows us to use the Bayesian framework previously developed without modifying the sampling and marginalization procedures of Jun *et al* (2005).

Thus, assuming that prior distributions of location, orientation, time course and number of dipoles are independent of the skull conductivity, our formulation of the Bayesian inference has the form

$$P(N, \mathbf{R}, \boldsymbol{\Theta}, \mathbf{J}, \mathbf{C}, \sigma_{\text{skull}}|\mathbf{E}) \propto P(\mathbf{E}|N, \mathbf{R}, \boldsymbol{\Theta}, \mathbf{J}, \mathbf{C}, \sigma_{\text{skull}}) \times P(\boldsymbol{\Theta}|\mathbf{R}, N)P(\mathbf{J}|N)P(\mathbf{R}|N)P(N)P(\mathbf{C})P(\sigma_{\text{skull}}). \tag{17}$$

Due to the clever separation of parameters, expression (17) utilizes all derivations of Jun *et al* (2005). The only thing introduced to the formulation is the prior probability of σ_{skull}. After applying marginalization over $\mathbf{J}$ and noise covariance $\mathbf{C}$, the final posterior distribution becomes

$$P_{\tilde{\mathbf{J}}}(N, \mathbf{R}, \boldsymbol{\Theta}, \sigma_{\text{skull}}|\mathbf{E}). \tag{18}$$

To complete the formulation we need to set a functional form of the prior distribution on the skull conductivity. With a wide spread of σ_{skull} values reported in the literature (Akhtari *et al* 2002, Hoekema *et al* 2003, Oostendorp *et al* 2000, Baysal and Haueisen 2004) it is hard to extract a definite pattern of more and less likely conductivities in order to make an informed choice for such a distribution. Instead we chose to allow skull conductivity to vary in the whole range of reported possible conductivity values $[\sigma_{\min} \ldots \sigma_{\max}]$ without preferring any particular one, i.e., we chose a uniform prior:

$$P(\sigma_{\text{skull}}) = \frac{1}{\sigma_{\max} - \sigma_{\min}}. \tag{19}$$

The complete probabilistic description of the problem and construction of the posterior is the first step in Bayesian inference. The next step is to extract a representative sample of likely solutions from the posterior distribution using a MCMC sampling technique. From the set of sampled likely solutions, we can infer statistical information about any feature of these solutions. This provides an effective means for quantifying uncertainty that is distinct from the other approaches to uncertainty quantification in inverse algorithms (Medvick *et al* 1989, Singh and Harding 2000, Darvas *et al* 2005).

3.3. Interpolation scheme

After sampling σ_{skull}, the large matrix portion of equation (16), enclosed in parentheses, must be inverted. Because of this required inversion, there may not be any computational advantages over FEM. To lessen the computing burden and overcome the problem, we introduce the following algorithm:

- Choose the range of possible values for $\sigma_{\text{skull}} - [\sigma_{\min} \ldots \sigma_{\max}]$.
- Discretize it with mesh step h_σ.
- Precompute the inverse in (16) for the value of σ_{skull} at each step.
- In MCMC procedure, draw a sample of σ_{skull} from a chosen prior probability density and find the closest smaller and larger values in the discretized range.
- Calculate solutions for both of these values.
- Interpolate to get the value at the drawn σ_{skull}.

The approach allows us to avoid extensive precomputation. Only a finite number of matrices need to be precomputed. The required number is realistic and easily manageable, as we demonstrate in section 4. At the same time, it provides a consistent way to complete the values in those parts of the range where no precomputation has been performed. The result is a continuous sampling in the space of the skull conductivity.

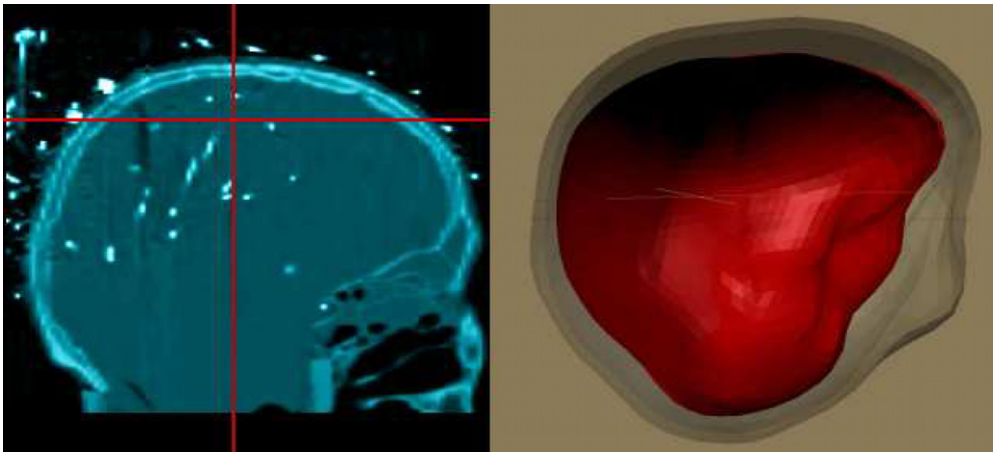

Figure 2. A CT scan slice with dipole sources and electrodes visible (left panel) and a smooth 3-shell tesselation model used in this work (right panel).

4. Experimental results

In Leahy *et al* (1998) a localization accuracy study was performed using a human skull phantom. The experiment is attractive to our work because all influence of the head except that of the skull is eliminated. Only the skull is real, the 'scalp' is latex and the brain cavity is filled with gel of known conductivity. Furthermore, the signal was generated by coaxial cables constructed to produce dipolar current and the location of these cables was extracted from a CT scan of the phantom. A CT scan slice with clearly visible cables and electrodes is shown in figure 2. A triangular mesh for the model was obtained by the authors of Leahy *et al* (1998) by segmentation of the CT scan. A modified version of this mesh is used in our experiments—it has been smoothed and some inconsistencies have been corrected (see figure 2). For the evaluation of the performance of our probabilistic model we use the data of the skull phantom study.

4.1. Simulated data

In order to control the performance of the algorithm and create a simple case with a known outcome, we have generated simulated data using the mesh of the human head phantom and source locations at the real dipole positions with sinusoidal time courses. Following the recommendations of Akhtari *et al* (2002) and of Hoekema *et al* (2003), table I, but allowing greater variability for σ_{skull}, we have set the possible conductivity range to [0.002, 0.082] S m^{-1} and have generated simulated data using the value of 0.004 S m^{-1}.

Using results of the calculation for one of the dipoles we demonstrate the convergence properties of our sampling. The MCMC run was conducted for 10 000 iterations and figure 3 contains a plot of log of the posterior probability, where the long lasting variations around the value of -3220 indicate the convergence of the process. Similar steady state behavior was observed for the other dipoles.

Posterior distribution for the location components is shown in figure 4, where a black vertical line denotes the true solution. The figure demonstrates that these distributions are consistent with the true location. An additional observation made here is that the variance of

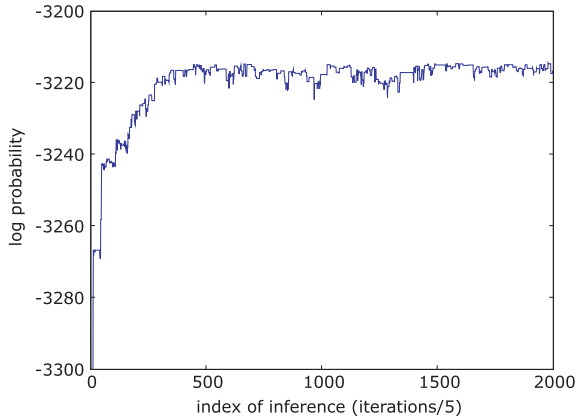

Figure 3. Log probability as a function of MCMC iterations for a simulated one dipole problem.

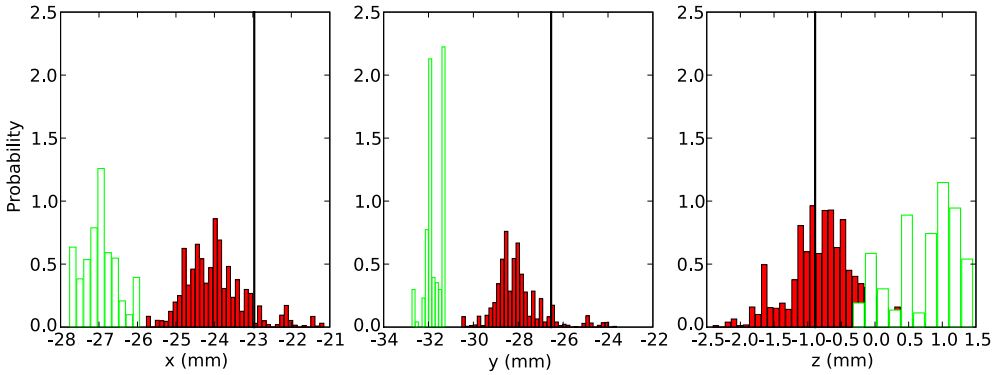

Figure 4. Location posterior distributions for one dipole from simulated data. True location is denoted by the black vertical lines. The result using the probabilistic forward model (solid color histogram) is closer to the true location and has larger variance compared to the conventional approach (outlined histogram).

the posteriors became bigger with the introduction of the probabilistic model. We demonstrate the effect on phantom data in figure 6.

4.2. Human skull phantom data

The posterior distribution of MEG source analysis is, in general, more consistent with correct dipole locations and the EEG source analysis posterior location distribution is inconsistent with the expected outcome. It is impossible to perform the joint analysis with two non-overlapping distributions as the result will be a null distribution. That is, these distributions are inconsistent with the hypothesis that both MEG and EEG come from the same single source. The explicit accounting of the uncertainty provided by the probabilistic forward model can resolve the problem of combining MEG and EEG in joint analysis. Such analysis can bring EEG results closer to the true locations or can widen the EEG location posterior distribution or both. Increase in the variance is as good for the purpose of improving consistency as moving the

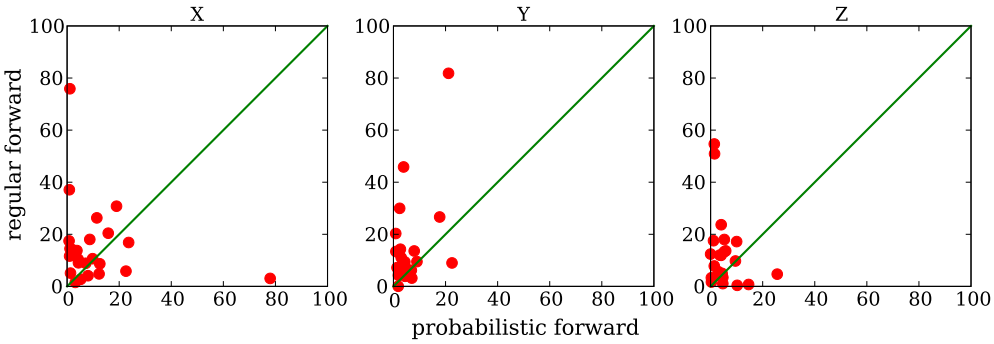

Figure 5. Scatterplots of χ for each axis a. The smaller values are better. The points above the 45° line mean that the probabilistic forward model performed better according to χ.

mean closer to the true location. Both of these changes make the dipoles that were very unlikely according to EEG posterior very likely, thus making combination with MEG results beneficial. In order to summarize both these changes as one number, we use the following criterion. Given that the mean of the posterior distribution is x, its standard deviation is σ and the true value is $\bar{x}$, we establish a criterion:

$$\chi = \frac{|x - \bar{x}|}{\sigma}. \tag{20}$$

Minimization of this criterion results in improving consistency of EEG sampling and increasing opportunities for joint MEG/EEG analysis.

In order to evaluate the probabilistic model, we have used the data of the human skull phantom experiment (Leahy *et al* 1998) and performed Bayesian analysis for each dipole using the conventional approach with fixed σ_{skull} set to 0.0042 Sm^{-1} and using our new probabilistic forward model allowing σ_{skull} to vary in the same range as for the simulated experiment. The results for 24 dipoles are summarized in figure 5. We show scatter plots for each dimension of the conventional model across probabilistic model results. The scatter plots illustrate which approach produces the smaller criterion. The points above the 45° line mean that the probabilistic forward model performed better according to χ.

An example of results for one of the dipoles is shown in figure 6. It compares posterior distributions of locations for each dimension for the conventional method, when σ_{skull} is fixed, with one using the probabilistic forward model. The new results (in red in the electronic version of the journal) are wider and closer to the true location (black vertical lines). Thus, the probabilistic forward model makes location posterior distributions consistent with the underlying dipole locations. This comes as an effect of propagating skull conductivity uncertainty to the results of source analysis.

In light of the Cramer–Rao bound results obtained in section 2, it is interesting to look at how the skull conductivity is sampled. There was no known true skull conductivity in this experiment since a real skull was used whose conductivity is not uniform nor known *a priori*. For the starting point of the conductivity estimate a random value was used. The sampling of the allowable range is presented in figure 7. As the left plot shows, MCMC has sampled the whole range achieving a good coverage of possible values. Some preferable values of σ_{skull} are visible in the histogram on the right. This is consistent with the CRLB demonstrating that any value of σ_{skull} in the range is almost equally likely.

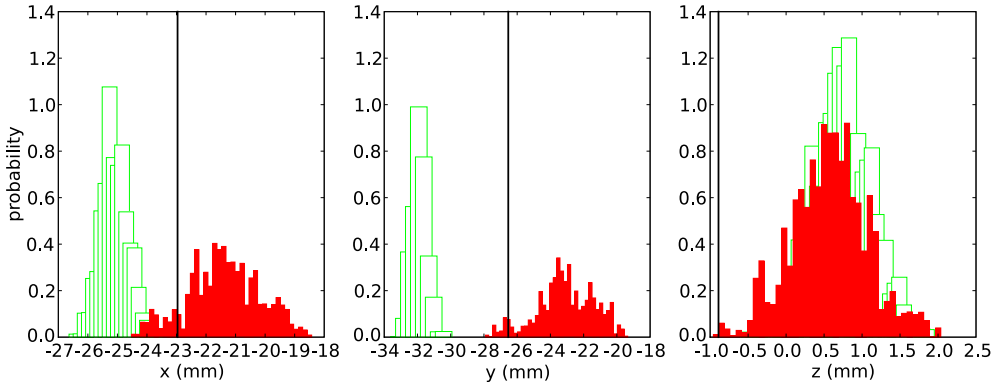

Figure 6. Comparison of location posteriors for one of the dipoles using two methods: one with the probabilistic forward model (shaded histogram) and the other—the conventional approach (outlined histogram). The probabilistic model result is consistent with the source location (the black vertical lines) and has higher variance.

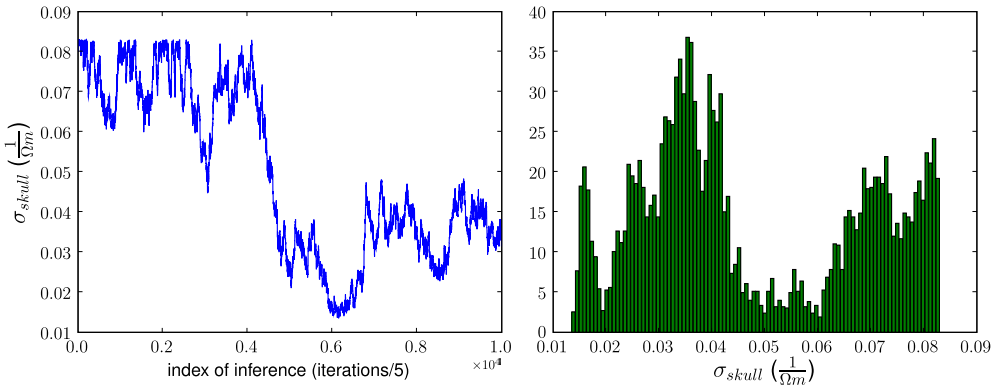

Figure 7. Skull conductivity sampling on each fifth MCMC iteration (on the left) and the posterior distribution of this conductivity (on the right).

5. Discussion

The idea of extracting the skull conductivity directly from the EEG data has been suggested by several researchers (Gutierrez *et al* 2004, Lew *et al* 2007, Vallaghé *et al* 2007). However, previous studies employed constrained estimation. In Gutierrez *et al* (2004), known source locations were assumed; in Vallaghé *et al* (2007) the investigator found that constraints are necessary in order to limit the space of possible dipole locations in order to achieve reliable results. In Lew *et al* (2007), only a small set of allowable values of the skull conductivity was used. Section 2 explains the observations made in these works by rigorous calculations of the CRLBs. We show that when adding skull conductivity as a model parameter to be fit, the Cramer–Rao bound increases for the location parameters making them more uncertain. Although the model is calculated analytically for the case of the spherical head model, its effects are also apparent on a realistic head model. In order to demonstrate the consequences of our computations of the CRLB, we have used the 3-shell mesh and 32 dipole locations

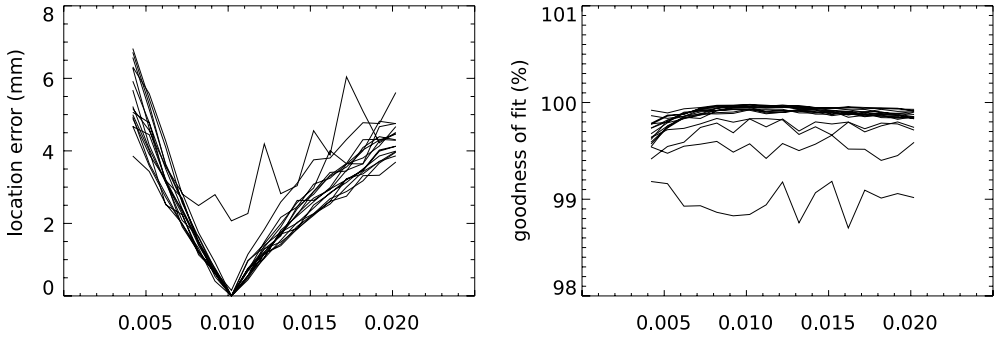

(a) Location error (b) Goodness of fit

Figure 8. Location error and the corresponding goodness of fit values for 32 single dipole problems simulated with the skull conductivity value set to $0.01021/(\Omega\,\mathrm{m})$ but analyzed with different fixed values of skull conductivity.

from Leahy *et al* (1998) as shown of figure 2 in order to generate 32 noiseless single-dipole problems with the skull conductivity set to $0.0102\,1/(\Omega\,\mathrm{m})$. For each of these problems we found an optimal solution in terms of the normalized goodness of fit for each of the values of skull conductivity from the range $[0.0042\,1/(\Omega\,\mathrm{m}), 0.0202\,1/(\Omega\,\mathrm{m})]$ with a step size of $0.001\,1/(\Omega\,\mathrm{m})$. For the target function we have used a normalized goodness of fit expressed as

$$\left(1 - \frac{\|\boldsymbol{E} - \boldsymbol{E}_M\|^2}{\|\boldsymbol{E}_M\|^2}\right) \cdot 100, \tag{21}$$

where $\boldsymbol{E}_M$ is the EEG measurements and $\boldsymbol{E}$ is the result after the forward calculation. The results of this simulation are presented in figure 8. The figure shows that for a wide variation of the location for each of the 32 dipoles the normalized goodness of fit stays practically flat. Even though there is some variation with the maximum at the true conductivity value, all this variation falls within 1%, as clearly visible in figure 8(b). Considering that these results are from the noiseless case, it is clear that optimization in real settings is impractical.

Based on these findings, we conclude that an external procedure of estimating the skull conductivity is needed. This can be accomplished through EIT (Salman *et al* 2005, Tidswell *et al* 2001, Glidewell and Ng 1997). Since the uncertainty is not completely eliminated even with separate measurement setups, the estimate obtained in such a method should be used as a mean value of the prior of the probabilistic model with some assumed form of the distribution.

Improvements in the consistency of EEG posteriors with the true dipole location should improve the results of a combined MEG and EEG analysis. One possible improvement, besides better dipole parameters estimation, is enhanced estimation of the skull conductivity. We expect that a CRLB analysis similar to the one presented here but with the addition of MEG data will show improved results for σ_{skull}. MEG should constrain the locations and force the analysis to optimize the skull conductivity. For example, figure 7 demonstrates that in EEG-only analysis σ_{skull} is sampled all over the allowable space without a pronounced preference towards a single value. We expect that in the joint analysis, the posterior distribution of σ_{skull} will be more peaked around its true value.

Modeling the skull conductivity as a random variable naturally incorporates the uncertainty into the forward calculation and accounts for the effect of inhomogeneities of

conductivity to randomly affecting results of forward calculations. Skull conductivity has a nonlinear effect on the solution and by modeling it with a random variable we try to account for that effect and obtain confidence limits. Even though the diploic structure of the skull and its influence on the surface potential distribution is deterministic, it is legitimate to model it as random quantity since we do not know the proper value. The uncertainties introduced by the impossibility of correctly measuring all fine details of tissue geometry and conductivity profile, the inter- and intra-subject variability and difficulties with the numerical issues associated with detailed geometrical models make the probabilistic approach an attractive alternative.

The probabilistic forward model is not limited to modeling the single parameter of skull conductivity. Other parameters of the forward model that are inherently uncertain can be modeled with our approach. For example, it is possible to extend the probabilistic forward model to account for the anisotropy of the skull. The skull is more conducting in the tangential direction and less conducting in the radial one. This property can be modeled by adding two additional shells into the skull volume of the 3-shell model used in this work. This could be accomplished by either two additional concentric shells or one shell inside the skull volume. It would slow down the computation because of the increase in the number of discretization points. However, this is not a dramatic effect except for the pre-computing time since the actual forward calculation time can be sufficiently decreased using the ideas of Mosher *et al* (1999). An additional parameter to the current probabilistic model would increase the sampling complexity but one parameter is not a terrible price to pay for the increase in descriptive power and improvement in realism of the model. A BEM method that suits this approach the best is symmetric BEM (Adde *et al* 2003). The relatively small sensitivity to mesh size perturbations and distances between the shells makes it attractive for the case where four shells need to be fitted in a small space. Other BEM methods would inevitably be affected by this setup. A preliminary study, where a high conductivity layer was added to the skull layer in the spherical head model, demonstrated an effect similar to the one shown in Wolters *et al* (2006), figure 8. Another possible approach to modeling random conducting media can be adopted from Fokin (1996).

The importance of the skull's influence on the forward computation was shown by Hämäläinen and Sarvas (1989), Leahy *et al* (1998), Wolters *et al* (2006). In a setup with no influence from other tissue but the skull we have demonstrated that accounting for the uncertainty by using a probabilistic model made results more consistent with the true solutions. Accounting for anisotropy in the way discussed above can make results more realistic but should not change the demonstrated effect. The importance of using a probabilistic forward model for EEG should be realized also for the brain tissue in order to extend it to the analysis of data from human subjects. Even in its present form, our approach can be used on real data to model the skull influence, which is the dominant effect on EEG source localization. However, a whole head probabilistic model, with only a few parameters in order not to overly complicate the sampling in MCMC, would be beneficial for human data analysis.

6. Conclusions

This work introduces a notion of a probabilistic forward model as a means to account for the effect of the uncertainties in the forward model on source analysis results. We have demonstrated the utility of this model by treating the uncertainties in the skull conductivity and showing how this strategy can be useful in joint MEG and EEG source analysis. The importance of treating skull conductivity as an uncertain parameter of the probabilistic model is highlighted by another result demonstrated here; the impossibility of improving source analysis results by treating the skull conductivity as a parameter to be fitted based on the

physiological data. We have demonstrated a dramatic increase in the CRLB when the skull conductivity parameter is added to the analysis. The Cramer–Rao bound results demonstrate the necessity of estimating skull conductivity in a separate procedure. Due to the nature of the skull structure some uncertainties will remain and the use of a probabilistic forward model can account for the effects of these uncertainties.

Acknowledgments

This work was supported by NIH grant 2 R01 EB000310-05 and the Mental Illness and Neuroscience Discovery (MIND) Institute. Sergey Plis was supported in part by NIMH grant number 1 R01 MH076282-01 as part of the NSF/NIH Collaborative Research in Computational Neuroscience Program. The authors thank John Mosher for fruitful discussions regarding the CRLB and the boundary element method.

Appendix A. Calculation of the Cramer–Rao lower bound

The CRLB derivation presented in this section is based on Stoica and Nehorai (1989) and Mosher *et al* (1993). We adopt the notation used in (Mosher *et al* 1993) and use a derivation obtained in Appendix E of Stoica and Nehorai (1989). We only consider the case where a single dipole is used. This is sufficient for the purpose of our paper and can be easily generalized to the multi-dipole case if necessary. In this case the vector of free parameters as used in both of the papers is

$$\psi = [\nu, \boldsymbol{q}^T, \boldsymbol{I}^T]^T, \tag{A.1}$$

where ν is the noise variance, $\boldsymbol{q}$ is the dipole moment vector and $\boldsymbol{I}$ is the dipole location vector.

In order to consider the feasibility of adding optimization parameter σ_{skull} to the analysis, we add it to vector (A.1), which then becomes

$$\psi = [\nu, \boldsymbol{q}^T, \boldsymbol{I}^T, \sigma_{\text{skull}}]^T. \tag{A.2}$$

We next need to calculate the changes in the Fisher information matrix introduced by adding the parameter. The gain matrix $\boldsymbol{G}$ nonlinearly depends on σ_{skull} as it does on the location vector $\boldsymbol{I}$. The derivative of the log likelihood with respect to a nonlinear parameter ω_i is expressed (Stoica and Nehorai 1989) as

$$\frac{\partial \ln L}{\partial \omega_i} = \frac{2}{\sqrt{\nu}} \sum_{t=1}^{N} \boldsymbol{q}^T(t) \frac{\partial \boldsymbol{G}^T}{\partial \omega_i} e(t), \tag{A.3}$$

where $e(t)$ is the uncorrelated additive noise. Replacing ω_i with σ_{skull}, we rewrite

$$\frac{\partial \ln L}{\partial \sigma_{\text{skull}}} = \frac{2}{\sqrt{\nu}} \sum_{t=1}^{N} \boldsymbol{q}^T(t) \frac{\partial \boldsymbol{G}^T}{\partial \sigma_{\text{skull}}} e(t). \tag{A.4}$$

We next derive the elements of the Fisher information matrix that appear when introducing σ_{skull}. For this, we need to define $\boldsymbol{D}$ as the partials of the gain matrix $\boldsymbol{G}$,

$$\boldsymbol{I} = [x, y, z] \qquad \boldsymbol{d}(x) = \frac{\partial}{\partial x} \boldsymbol{G}(\boldsymbol{I}) \qquad \boldsymbol{D} = [\boldsymbol{d}(x), \boldsymbol{d}(y), \boldsymbol{d}(z)], \tag{A.5}$$

and define $\boldsymbol{X}$ as a block-diagonal matrix of the moment $\boldsymbol{q}$:

$$\boldsymbol{X}(t) = \mathbf{I} \otimes \boldsymbol{q}(t). \tag{A.6}$$

Using definitions (A.5) and (A.6), the Fisher information matrix elements are obtained as

$$E\left[\frac{\partial \ln L}{\partial \boldsymbol{q}(k)}\right]\left[\frac{\partial \ln L}{\partial \sigma_{\text{skull}}}\right]^T = \frac{2}{\nu}E\left(\boldsymbol{G}^T e(k)e^T(t)\frac{\partial \boldsymbol{G}}{\partial \sigma_{\text{skull}}}\boldsymbol{q}(t)\right)$$
$$= \frac{2}{\sqrt{\nu}}\boldsymbol{G}^T\frac{\partial \boldsymbol{G}}{\partial \sigma_{\text{skull}}}\boldsymbol{q}(t) \tag{A.7}$$

$$E\left[\frac{\partial \ln L}{\partial \boldsymbol{I}(k)}\right]\left[\frac{\partial \ln L}{\partial \sigma_{\text{skull}}}\right]^T = \frac{2}{\nu}E\left(\sum_{t=1}^{N}\sum_{t=1}^{N}\boldsymbol{X}^T(t)\boldsymbol{D}^T e(t)e^T(t)\frac{\partial \boldsymbol{G}}{\partial \sigma_{\text{skull}}}\boldsymbol{q}(k)\right)$$
$$= \frac{2}{\sqrt{\nu}}\sum_{t=1}^{N}\boldsymbol{X}^T(t)\boldsymbol{D}^T\frac{\partial \boldsymbol{G}}{\partial \sigma_{\text{skull}}}\boldsymbol{q}(t) \tag{A.8}$$

$$E\left[\frac{\partial \ln L}{\partial \sigma_{\text{skull}}}\right]\left[\frac{\partial \ln L}{\partial \sigma_{\text{skull}}}\right]^T = \frac{2}{\nu}E\left(\sum_{t=1}^{N}\sum_{t=1}^{N}\boldsymbol{q}^T(k)\left(\frac{\partial \boldsymbol{G}}{\partial \sigma_{\text{skull}}}\right)^T e(k)e^T(t)\frac{\partial \boldsymbol{G}}{\partial \sigma_{\text{skull}}}\boldsymbol{q}(t)\right)$$
$$= \frac{2}{\sqrt{\nu}}\sum_{t=1}^{N}\boldsymbol{q}^T(t)\left(\frac{\partial \boldsymbol{G}}{\partial \sigma_{\text{skull}}}\right)^T\frac{\partial \boldsymbol{G}}{\partial \sigma_{\text{skull}}}\boldsymbol{q}(t). \tag{A.9}$$

For our purposes it suffices to look at a single time point and compare the CRLB of analysis that uses σ_{skull} as an additional parameter with the analysis that uses a fixed σ_{skull} value. Dropping time indices, we define the following matrices:

$$\Gamma = \boldsymbol{X}^T\boldsymbol{D}^T\boldsymbol{D}\boldsymbol{X} \tag{A.10}$$
$$\Delta = \boldsymbol{G}^T\boldsymbol{D}\boldsymbol{X}. \tag{A.11}$$

The Fisher information matrix for the parameter vector (A.1) as derived in Mosher *et al* (1993), Stoica and Nehorai (1989) is expressed as

$$\boldsymbol{J} = \frac{1}{\nu}\begin{bmatrix}\frac{m}{2\nu} & 0 & 0\\ 0 & \mathbf{G}^T\mathbf{G} & \Delta\\ 0 & \Delta^T & \Gamma\end{bmatrix}. \tag{A.12}$$

Denoting the covariances derived in (A.7) as

$$S = \boldsymbol{q}^T\left(\frac{\partial \boldsymbol{G}}{\partial \sigma_{\text{skull}}}\right)^T\frac{\partial \boldsymbol{G}}{\partial \sigma_{\text{skull}}}\boldsymbol{q}$$
$$\alpha_\Delta = \boldsymbol{G}^T\frac{\partial \boldsymbol{G}}{\partial \sigma_{\text{skull}}}\boldsymbol{q} \tag{A.13}$$
$$\beta_\Gamma = \boldsymbol{X}^T\boldsymbol{D}^T\frac{\partial \boldsymbol{G}}{\partial \sigma_{\text{skull}}}\boldsymbol{q},$$

we define the Fisher information matrix for parameter vector (A.2) as

$$\boldsymbol{J} = \frac{1}{\nu}\begin{bmatrix}\frac{m}{2\nu} & 0 & 0 & 0\\ 0 & \boldsymbol{G}^T\boldsymbol{G} & \Delta & \alpha_\Delta\\ 0 & \Delta^T & \Gamma & \beta_\Gamma\\ 0 & \alpha_\Delta^T & \beta_\Gamma^T & S\end{bmatrix}. \tag{A.14}$$

The CRLB of a parameter can be calculated from the inverse of this matrix by taking its corresponding diagonal element. For this extended case we can either invert the lower block of the matrix without the first column and the first row or we can use partitioned matrix inversion, as was done in Mosher *et al* (1993).

References

Adde G, Clerc M, Faugeras O, Keriven R, Kybic J and Papadopoulo T 2003 Symmetric BEM formulation for the M/EEG forward problem *Proc. of Information Processing in Medical Imaging (Lecture Notes in Computer Science)* vol 2732 (Berlin: Springer) pp 524–35

Akhtari M *et al* 2002 Conductivities of three-layer live human skull *Brain Topogr.* **14** 151–67

Baysal U and Haueisen J 2004 Use of *a priori* information in estimating tissue resistivities—application to human data *in vivo Physiol. Meas.* **25** 737–48

Berg P and Scherg M 1994 A fast method for forward computation of multiple-shell spherical head models *Electroencephalogr. Clin. Neurophysiol.* **90** 58–64

Cuffin B N and Cohen D 1979 Comparison of the magneto encephalogram and electro encephalogram *Electroencephalogr. Clin. Neurophysiol.* **47** 132–46

Darvas F, Rautiainen M, Pantazis D, Baillet S, Benali H, Mosher J, Garnero L and Leahy R 2005 Investigations of dipole localization accuracy in MEG using the bootstrap *Neuroimage* **25** 355–68

Fokin A G 1996 Macroscopic conductivity of random inhomogeneous media. Calculation methods *Usp. Fiz. Nauk* **166** 1069–93

Gelman A, Carlin J B, Stern H S and Rubin D B 1995 *Bayesian Data Analysis* (London: Chapman and Hall)

Gilks W R 1995 *Markov Chain Monte Carlo in Practice* (London: Chapman and Hall)

Glidewell M E and Ng K T 1997 Anatomically constrained electrical impedance tomography for three-dimensional anisotropic bodies *IEEE Trans. Med. Imaging* **16** 572–80

Gutierrez D, Nehorai A and Muravchik C 2004 Estimating brain conductivities and dipole source signals with EEG arrays *IEEE Trans. Biomed. Eng.* **51** 2113–22

Hämäläinen M, Hari R, Ilmoniemi R, Knuutila J and Lounasmaa O 1993 Magnetoencephalography: theory, instrumentation, and applications to noninvasive studies of the working human brain *Rev. Mod. Phys.* **65** 413–97

Hämäläinen M S and Sarvas J 1989 Realistic conductivity geometry model of the human head for interpretation of neuromagnetic data *IEEE Trans. Biomed. Eng.* **36** 165–71

Hoekema R, Wieneke G H, Leijten F S S, van Veelen C W M, van Rijen P C, Huiskamp G J M, Ansems J and van Huffelen A C 2003 Measurement of the conductivity of skull, temporarily removed during epilepsy surgery *Brain Topogr.* **16** 29–38

Jun S C, George J S, Pare-Blagoev J, Plis S, Ranken D M, Schmidt D M and Wood C C 2005 Spatiotemporal Bayesian inference dipole analysis for MEG neuroimaging data *Neuroimage* **28** 84–98

Jun S C, George J S, Plis S M, Ranken D M, Schmidt D M and Wood C C 2006 Improving source detection and separation in spatiotemporal Bayesian inference dipole analysis *Phys. Med. Biol.* **51** 2395–414

Leahy R M, Mosher J C, Spencer M E, Huang M X and Lewine J D 1998 A study of dipole localization accuracy for MEG and EEG using a human skull phantom *Electroencephalogr. Clin. Neurophysiol.* **107** 159–73

Lew S, Wolters C H, Anwander A, Makeig S and MacLeod R S 2007 Low resolution conductivity estimation to improve source localization *New Frontiers in Biomagnetism. Proc. of the 15th Int. Conf. on Biomagnetism (International Congress Series)* pp 149–52

Liu A K, Dale A M and Belliveau J W 2002 Monte Carlo simulation studies of EEG and MEG localization accuracy *Hum. Brain Mapp.* **16** 47–62

Marin G, Guerin C, Baillet S, Garnero L and Meunier G 1998 Influence of skull anisotropy for the forward and inverse problem in EEG: simulation studies using FEM on realistic head models *Hum. Brain Mapp.* **6** 250–69

Medvick P A, Lewis P S, Aine C and Flynn E R 1989 Monte-Carlo analysis of localization errors in magnetoencephalography *Advances in Biomagnetism* ed S J Williamson, M Hoke, G Stroink and M Kotani (New York: Plenum) pp 543–6

Mosher J C, Leahy R M and Lewis P S 1999 EEG and MEG: forward solutions for inverse methods *IEEE Trans. Biomed. Eng.* **46** 245–59

Mosher J, Spencer M, Leahy R and Lewis P 1993 Error bounds for EEG and MEG dipole source localization *Electroencephalogr. Clin. Neurophysiol.* **86** 303–21

Ollikainen J O, Vauhkonen M, Karjalainen P A and Kaipio J P 1999 Effects of local skull inhomogeneities on EEG source estimation *Med. Eng. Phys.* **21** 143–54

Oostendorp T F, Delbeke J and Stegeman D F 2000 The conductivity of the human skull: results of *in vivo* and *in vitro* measurements *IEEE Trans. Biomed. Eng.* **47** 1487–92

Rush S and Driscoll D 1969 Electrode sensitivity: an application of reciprocity *IEEE Trans. Biomed. Eng.* **16** 15–22

Salman A, Turovets S, Malony A, Eriksen J and Tucker D 2005 Computational modeling of human head conductivity *Lecture Notes Comput. Sci.* **3514** 631–8

Sarvas J 1987 Basic mathematical and electromagnetic concepts of the biomagnetic inverse problem *Phys. Med. Biol.* **32** 11–22

Schmidt D M, George J S and Wood C C 1999 Bayesian inference applied to the electromagnetic inverse problem *Hum. Brain Mapp.* **7** 195–212

Singh K D and Harding G F A 2000 Monte-Carlo analysis and confidence region ellipsoids for equivalent current dipole solutions to EEG/MEG data *BIOMAG 96: Proc. 10th Int. Conf. on Biomagnetism* vols I and II ed C J Aine, Y Okada, G Stroink, S J Swithenby and C C Wood (Santa Fe, NM: Springer) pp 346–9

Stoica P and Nehorai A 1989 Music, maximum likelihood, and cramer-rao bound *IEEE Trans. Acoust. Speech Signal Process.* **37** 720–41

Strang G and Fix G J 1973 *An Analysis of the Finite Element Method* (Englewood Cliffs, NJ: Prentice-Hall)

Sun M 1997 An efficient algorithm for computing multishell spherical volume conductor models in EEG dipole source localization *IEEE Trans. Biomed. Eng.* **44** 1243–52

Tidswell T, Gibson A, Bayford R and Holder D 2001 Three-dimensional electrical impedance tomography of human brain activity *NeuroImage* **13** 283–94

Tuch D S, Wedeen V J, Dale A M, George J and Belliveau J W 2001 Conductivity tensor mapping of the human brain using diffusion tensor MRI *Proc. Natl Acad. Sci. USA* **98** 11697–701

Vallaghé S, Clerc M and Badier J-M 2007 *In vivo* conductivity estimation using somatosensory evoked potentials and cortical constraint on the source *4th IEEE Int. Symp. on Biomedical Imaging* pp 1036–9

Wolters C H, Anwander A, Tricoche X, Weinstein D, Koch M A and MacLeod R S 2006 Influence of tissue conductivity anisotropy on EEG/MEG field and return current computation in a realistic head model: a simulation and visualization study using high-resolution finite element modeling *NeuroImage* **30** 813–26